Numerical Simulations of Resonant Heat Transfer Augmentation at Low Reynolds Numbers

Miles Greiner
e-mail: greiner@unr.edu
ASME Member
Professor of Mechanical Engineering,
University of Nevada, Reno

Paul F. Fischer
e-mail: fischer@mcs.anl.gov
Mathematics and Computer Science Division,
Argonne National Laboratories

Henry Tufo
e-mail: hmt@cs.uchicago.edu
Department of Computer Science,
University of Chicago

The effect of flow rate modulation on low Reynolds number heat transfer enhancement in a transversely grooved passage was numerically simulated using a two-dimensional spectral element technique. Simulations were performed at subcritical Reynolds numbers of $\mathrm{Re}_m = 133$ *and 267, with 20 percent and 40 percent flow rate oscillations. The net pumping power required to modulate the flow was minimized as the forcing frequency approached the predicted natural frequency. However, mixing and heat transfer levels both increased as the natural frequency was approached. Oscillatory forcing in a grooved passage requires two orders of magnitude less pumping power than flat passage systems for the same heat transfer level. Hydrodynamic resonance appears to be an effective method of increasing heat transfer in low Reynolds number systems, especially when pumping power is at a premium.* [DOI: 10.1115/1.1517273]

Keywords: Augmentation, Enhancement, Heat Transfer, Instability, Unsteady

Introduction

Miniaturization of electronic components has increased circuit junction density and the associated heat loads that must be removed to maintain reliable operation. New technologies allow micro-scale coolant passages to be cut directly into a variety of silicon circuit substrates. This technique reduces the thermal resistance between junctions and coolant passageways compared to ''strap-on'' heat sink techniques. Moreover, the small dimensions of the passages lead to very large heat transfer coefficients even at low Reynolds numbers [1,2].

The small surface area and lack of convective mixing associated with micro-channels are a limitation to their heat transfer performance. Fins, offset strips and jet array impingement are routinely used to increase convection in full-sized devices [3]. However, these features are subject to fouling and manufacturability problems in micro-scale systems. Moreover, they require the use of more powerful prime movers, which may be problematic in micro-devices. Finally, these techniques are not specifically designed to enhance convective mixing.

In recent years, a number of researchers have considered passage configurations that enhance mixing and heat transfer by triggering flow instabilities. Transversely grooved channels [4–6], passages with eddy promoters [7,8] and communicating channels [9] all contain features whose sizes are roughly half the channel wall to wall spacing. These structures excite normally damped Tollmien-Schlichting waves at moderately low Reynolds numbers.

The current authors have presented a series of studies on flow destabilization in rectangular cross section channels with transverse grooves cut periodically into the walls. Visualizations in a range of passage geometries show that the critical Reynolds number Re_C where two-dimensional waves first appear decreases as the spacing between grooves is reduced [10]. For a sawtooth-shaped wall with no spacing between grooves, two-dimensional waves first appear at $\mathrm{Re}_C = 350$, followed by a rapid transition to three-dimensional mixing [11]. Fully developed heat transfer using air is enhanced relative to laminar flat channel flow by as much as a factor of 4.6 at equal Reynolds numbers and by a factor of 3.5 *at equal pumping powers* [12–15].

Numerical and experimental studies of hydrodynamic resonance show that Tollmien-Schlichting waves may also be triggered *below* the critical Reynolds number by modulating the flow rate at the natural frequency of the waves [4,5,16]. Experiments and simulations were performed for *sparsely* grooved passages in which two-dimensional waves first appeared at $\mathrm{Re}_C = 2000$ (the onset of three-dimensional mixing in a flat passage occurs at $\mathrm{Re}_m = 2800$ [17]. At a subcritical Reynolds number of $\mathrm{Re}_m = 1400$ ($\mathrm{Re}_m/\mathrm{Re}_C = 0.7$), a 20 percent flow rate modulation at the correct frequency more than doubled the heat transfer.

Problem Definition

The goals of the current paper are to (*a*) determine if resonant heat transfer augmentation provides significant enhancement at the low Reynolds numbers where micro-channels typically operate [1,2], and (*b*) compare the pumping power required to effect a given heat transfer level by steady forcing and modulated flow. In this work, numerical simulations are performed in the rectangular cross section passage with sawtooth walls shown in Fig. 1. The minimum and maximum wall-to-wall spacing are $H_{\min} = 0.01$ m and $H_{\max} = 0.034$ m respectively, and the groove length is $L = 0.024$ m. This geometry was chosen because it has a critical Reynolds number of $\mathrm{Re}_C = 350$, which is the lowest value of any geometry examined by Greiner [10]. The large dimensions of the current study were chosen as a practical size for future bench-scale experiments that will be performed to validate the simulation results. Typical micro-scale dimensions are much smaller.

We choose the *mean* wall-to-wall spacing as the characteristic dimension for this passage, $H = (H_{\min} + H_{\max})/2$, with a corresponding hydraulic diameter of $D_h = 2H$. This allows the results of the current study to be directly compared to a flat passage whose wall-to-wall spacing is equal to the mean spacing of the current grooved passage. The volume of the flat passage is also equal to that of the grooved channel.

The coolant for this study is modeled as constant-property room temperature air with thermal conductivity k, density ρ, thermal diffusivity α_t, molecular Prandtl number Pr, and kinematic vis-

Contributed by the Heat Transfer Division for publication in the JOURNAL OF HEAT TRANSFER. Manuscript received by the Heat Transfer Division October 22, 2001; revision received August 12, 2002. Associate Editor: M. Faghri.

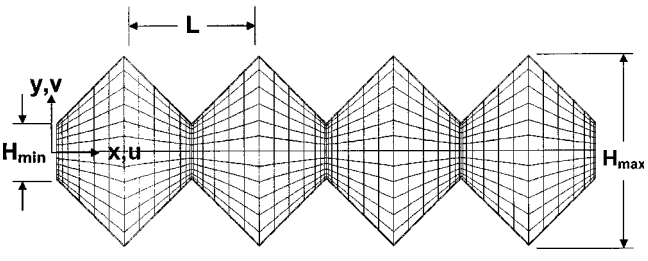

Fig. 1 Spectral Element Mesh. The flow is from left to right and periodic inlet/outlet conditions are employed.

cosity ν. The working fluid flows from left to right in Fig. 1. Its volumetric flow rate per unit length normal to the plane of Fig. 1, $V_N(t)=\int u dy$, is modulated sinusoidally with time. The time dependent Reynolds number based on hydraulic diameter D_h is

$$\mathrm{Re}(t)=\frac{U_m(t)D_h}{\nu}=V_N(t)\frac{2}{\nu}=\mathrm{Re}_m[1+\eta\sin(2\pi Ft)] \quad (1)$$

In this expression, time dependent mean velocity is $U_m(t)=V_N(t)/H$, Re_m is the time mean Reynolds number, η is the oscillatory fraction, and F is the forcing frequency.

In this work, simulations are performed for two subcritical Reynolds numbers $\mathrm{Re}_m=133$ and 267, corresponding to ratios of mean to critical Reynolds numbers of $\mathrm{Re}_m/\mathrm{Re}_C=0.38$ and 0.76, respectively. The higher of these ratios is roughly the same as that studied by Ghaddar et al. [4] and Greiner [5] at $\mathrm{Re}_m=1400$. The lower Reynolds number is deeply in the subcritical range. Simulations are performed for oscillatory fractions $\eta=0$ (steady forcing), 0.2 and 0.4, and a range for forcing frequencies, F.

In the next section, linear stability results for a *flat* passage are used to estimate the forcing frequency that maximizes the heat transfer in the current *grooved* channel. We perform numerical simulations for a range of forcing frequencies centered about the predicted natural frequencies and determine the effect on heat transfer and time average pumping power.

Linear Stability of Plane Poiseuille Flow

Linear stability analysis of flat passage flow is generally used to determine if certain infinitesimal perturbations grow, decay, or remain unchanged with time [18]. Linear perturbations to plane Poiseuille flow are generally composed of traveling waves with a range of wavelengths λ. All *two*-dimensional perturbations to laminar flat passage flow decay below a critical Reynolds numbers of $\mathrm{Re}_C=U_mD_h/\nu=15{,}392$ (the well-known Orr-Sommerfeld value of $\mathrm{Re}_{C,OS}=U_{\max}h/\nu=5772$ is based on the channel half height $h=H/2$ and the maximum fluid velocity $U_{\max}=(3/2)U_m$, so that $\mathrm{Re}_{C,OS}=3/8\ \mathrm{Re}_C$). However, *three*-dimensional *finite*-amplitude perturbations first grow at a lower Reynolds number of $\mathrm{Re}_m=2800$ and this begins the transition to turbulence.

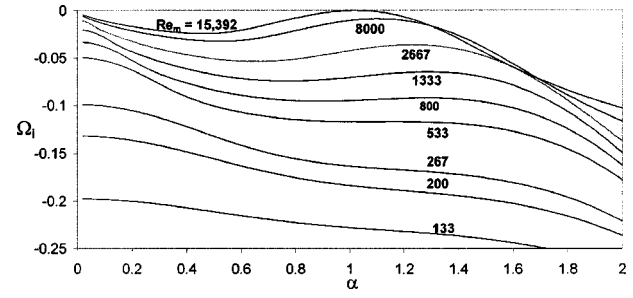

Fig. 2 Orr-Sommerfeld growth rate versus wavenumber and Reynolds number

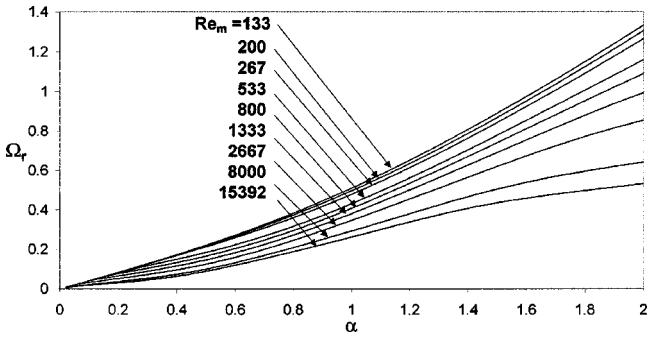

Fig. 3 Orr-Sommerfeld frequency versus wavenumber and Reynolds number

At any location within a plane passage the amplitude of each perturbation wave varies with time t according to $e^{Gt}\sin(2\pi Ft)$, where G is its dimensional growth rate and F is its dimensional natural frequency. The values of G and F for different perturbation wavelengths and Reynolds numbers are found from solutions to the Orr-Sommerfeld linearized equation of motion. Figures 2 and 3 show dimensionless growth rate $\Omega_i=2\pi GH/(3U_m)$ and dimensionless natural frequency $\Omega_r=2\pi FH/(3U_m)$ versus dimensionless wavenumber $\alpha=\pi H/\lambda$ for a range of Reynolds numbers.

Figure 2 shows that at the critical Reynolds number $\mathrm{Re}_C=15{,}392$ and $\alpha=1.03$, the dimensionless growth rate is $\Omega_i=0$. This indicates that perturbations of wavelength $\lambda=\pi H/\alpha=3.05\,H$ are neutrally stable (neither grow nor decay). All disturbances for $\mathrm{Re}_m<\mathrm{Re}_C$ decay with time since they have negative growth rates. However, for $\sim 533<\mathrm{Re}_m<\mathrm{Re}_C$, each Reynolds number exhibits a maximum growth rate at wavenumbers between $1.03\leqslant\alpha\leqslant 1.3$. This indicates that certain wavelengths decay more slowly than the rest.

Ghaddar et al. [4] and Greiner [5] both studied resonant heat transfer enhancement at $\mathrm{Re}_m=1400$. This Reynolds number is in the range that exhibits a peak in the growth rate curve. The Reynolds number of interest in the current paper are $\mathrm{Re}_m=133$ and 267. Figure 2 shows that there are no peaks in the growth rate curves at these low Reynolds numbers. However, both curves are inflected (zero curvature) at $\alpha\cong 1.3$, and this appears to be the only remnant of the peaks observed at higher Reynolds numbers. This wavenumber corresponds to perturbation wavelength of $\lambda=\pi H/\alpha=2.4\,H$. The periodicity length of the current grooved passage $L=2.4\ H_{\min}$, was chosen to be compatible with this wavelength ($H_{\min}$ was chosen instead of H because the external channel flow with steady forcing moves essentially parallel to the x-direction, similar to an ungrooved passage). Figure 3 shows that at $\mathrm{Re}_m=133$ and 267, the dimensionless frequency for waves with $\alpha\cong 1.3$ are $\Omega_r=0.73$ and 0.69, respectively. The corresponding dimensional natural frequencies at $\mathrm{Re}_m=133$ and 267 are therefore $F_N=(3\Omega_r/2\pi)(U_m/H_{\min})=3\nu\Omega_r\,\mathrm{Re}/(4\pi H_{\min}^2)=4.24$ and 8.04 Hz, respectively.

Numerical Methods

Figure 1 shows the two-dimensional spectral element mesh employed in this work. The upper and lower boundaries are no-slip solid walls, and the flow is form left to right (in the positive x-direction). The domain consists of four grooves with a domain length $L_d=4\,L$. Periodic inlet/outlet conditions are employed to model fully developed flow. Multiple grooves are employed so that long wavelength modes, which may exist at low Reynolds numbers, will be observed. Heat transfer for constant temperature walls is modeled.

In the spectral element method [19,20] the velocity, data and geometry are expressed as tensor-product polynomials of degree N in each of K spectral elements, corresponding to a total grid point count of roughly KN^2. Numerical convergence is achieved

by increasing the spectral order N. The present calculations were carried out at a base resolution of $K=782$, $N=5$. Resolution tests with $N=7$ indicated a 0.096 percent change in Nusselt number at the resonant forcing condition for $\mathrm{Re}_m=267$.

The present simulations use consistent approximation spaces for velocity and pressure, with pressure represented as polynomials of degree N-2 [20,21]. The momentum equations are advanced by first computing the convection term, followed by a linear Stokes solve for the viscous and pressure terms. The decoupling allows for convective Courant numbers greater than unity while maintaining third-order accuracy in time. Full details of the method can be found in [21]. The flow is driven from left to right in the periodic domain by a time-varying body force per unit mass $f_x=(-dp/dx)/\rho$. This forcing is determined so that the mass flow rate through the domain varies sinusoidally with time [22].

The thermal problem for the periodic domain requires careful treatment. If one simply specifies zero-temperature conditions on the walls then the solution eventually decays to zero. To produce the desired spatially fully-developed state requires that the temperature profiles at the inlet and outlet be self-similar, that is, $T(x=L_d,y,t)=CT(x=0,y,t)$, with $T\geq 0$ and $C<1$. The solution technique for computing the fully developed temperature field for constant temperature boundary conditions follows the analysis of Patankar et al. [23]. The energy equation and associated initial and boundary conditions are

$$\frac{\partial T}{\partial t}+\overline{U}\cdot\nabla T=\alpha\cdot\nabla^2 T \tag{2a}$$

$$T(x,y,t=0)=T_{\mathrm{init}}(x,y) \tag{2b}$$

$$T(x,y,t)=0 \quad \text{on the walls} \tag{2c}$$

$$T(x=L_d,y,t)=e^{-cL_d}T(x=0,y,t) \tag{2d}$$

where $\overline{U}=(u,v)$ is the convecting velocity field determined by the hydrodynamic part of the computation. Equation (2d) corresponds to the fully developed condition where the temperature profile is self-similar in each successive domain in the periodic sequence, that is $T(x+L_d,y,t)=e^{-cL_d}\cdot T(x,y,t)$ for all (x,y,t), where $e^{-cL_d}=C$. The decay constant c is determined as part of the computation and is proportional to the log-mean Nusselt number. The fact that each domain independently satisfies the homogeneous Eq. (2) and that we are considering fully developed solutions that are independent of T_{init} implies that the solution to Eq. (2) for each domain would yield the same value of c. Hence, c cannot be a function of x. Moreover, since the log-mean Nusselt number is constant, c cannot be a function of time even when the flow is itself unsteady.

Any function satisfying the above self-similar condition has the unique decomposition $T(x,y,t)=e^{-cx}\theta(x,y,t)$, where $\theta(x+L_d,y,t)=\theta(x,y,t)$ is a periodic function. Thus, the computation of T is reduced to the computation of the periodic temperature function θ, and the constant c. Substituting this decomposition into Eq. 2 yields:

$$\frac{\partial\theta}{\partial t}+\overline{U}\cdot\nabla\theta-\alpha\cdot\nabla^2\theta=(\alpha\cdot c^2+uc)\theta-2\alpha\cdot c\frac{\partial\theta}{\partial x} \tag{3a}$$

$$\theta(x,y,t=0)=\theta_{\mathrm{init}}(x,y) \tag{3b}$$

$$\theta(x,y,t)=0 \quad \text{on the walls} \tag{3c}$$

$$\theta(x=L_d,y,t)=\theta(x=0,y,t) \tag{3d}$$

Since the fully developed solution is independent of the initial condition we may arbitrarily assign θ_{init}, which is typically set to unity when starting from rest, or to a prior converged result when starting from an existing flow-field. Equation (3a) is solved using a semi-implicit time-stepping procedure similar to that for our Navier-Stokes solver. The diffusive terms are treated implicity while the convective terms are treated explicitly. In addition, all terms on the right of Eq. (3a) are treated explicitly using the latest available value for c.

In the steady state case ($\partial/\partial t=0$), Eq. (3) constitutes an eigenproblem for the eigenpair (c,θ). The constant c corresponds to the decay rate of the mean temperature in the x-direction. As such, a larger value of c implies more rapid decay and more effective heat transfer (larger log-mean Nusselt number). In the convection-dominated limit where the Peclet number U_mD_h/α_t is large, Eq. (3a) becomes a linear eigenvalue problem. In this case, standard iterative methods for computing the lowest value of c (corresponding to the most slowly decaying mode in x) can be used even when the nonlinear (c^2) term in Equation (3a) is not identically zero. We find that this method accurately computes the decay rate and Nusselt numbers for steady flows in square and round ducts [24].

For steady-periodic flows with period τ, the temperature is periodic in time, implying $T(x,y,t+\tau)=T(x,y,t)$. Since c is independent of time, this implies that $\theta(x,y,t+\tau)=\theta(x,y,t)$. If the value of c is not chosen correctly, this condition will not be satisfied. A robust approach to computing c is obtained by multiplying Eq. (3a) by θ, integrating over the domain Ω, and simplifying to yield:

$$\frac{1}{2}\frac{d}{dt}\int_\Omega\theta^2 dV=\int_\Omega[(\alpha c^2+uc)\theta^2-\alpha\nabla\theta\cdot\nabla\theta]dV \tag{4}$$

While we do not expect the time derivative of the average temperature (represented by the left-hand side of Eq. (4)) to be identically zero, it will in general be less than the time derivative of θ at any one point in the domain. Moreover, if we integrate the right-hand side of Eq. (4) from time t to $t+\tau$, the resultant quantity must be zero due to the temporal periodicity.

This suggests a two-tier strategy for computing c in the unsteady case. Initially, we determine c such that the right hand side of Eq. (4) is identically zero at each time step. This permits a relatively coarse but quick determination of c and θ. We use this value of c to advance θ for one or more periods, and monitor the decay or growth of $\int\theta^2 dV$. At the end of each trial period, we adjust c until convergence is attained. Once the decay constant c has converged (typically about 15–20 periods), averages are taken over a single period. Simulation times for a single period are roughly 45 min on a two-processor 500 MHz DEC Alpha cluster.

The current numerical technique has been used to simulate highly unsteady three-dimensional flows at $\mathrm{Re}=1600$ in the same grooved passage under investigation in the present study [14]. The local and spatially averaged results from that study were in excellent agreement with experimental data. No experimental data for unsteadily forced flow in the current passage geometry are available to validate the results. However, because the Reynolds number is well below the values considered in our previous work, we are reasonably confident of the numerical technique's ability to accurately simulate the heat transfer in these flows.

Results

Figure 4 shows streamlines for $\mathrm{Re}_m=267$ and $\eta=0$ (no unsteady forcing). The critical Reynolds number for this passage is

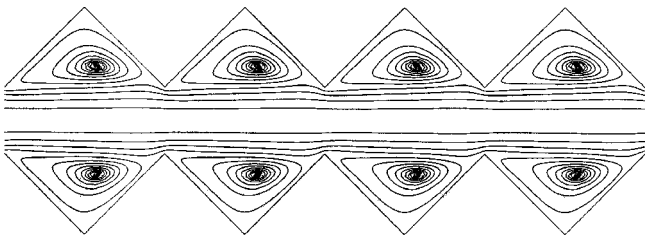

Fig. 4 Streamlines for Re=267, steady forcing

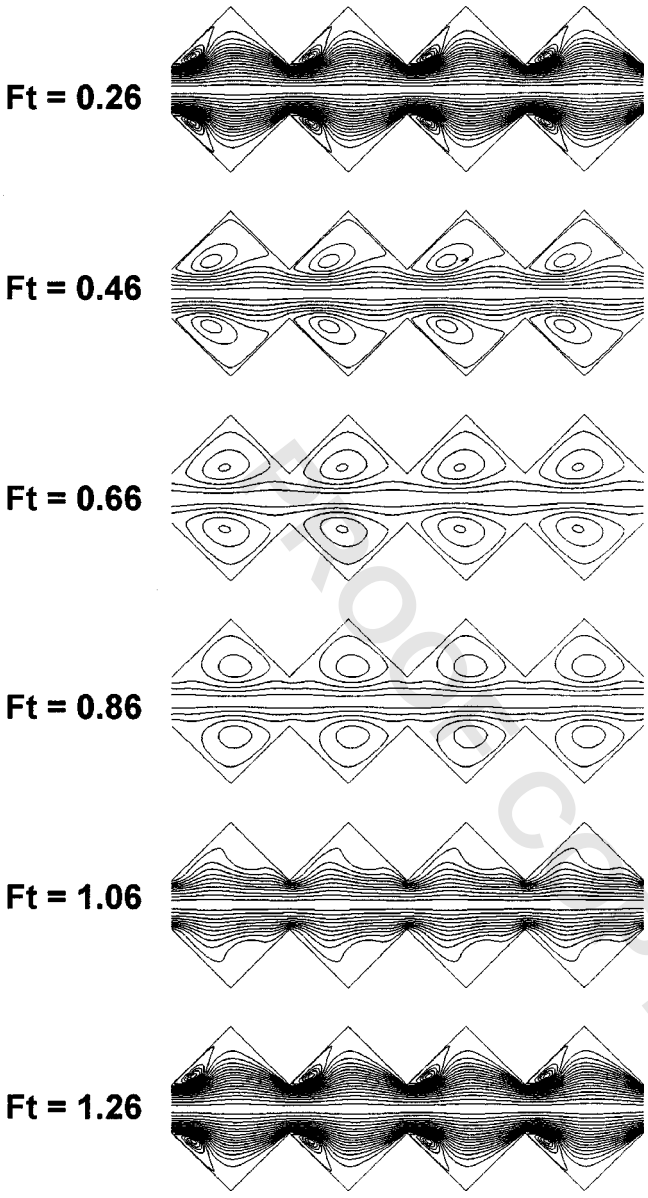

Fig. 5 Streamlines for Re=267, η=0.4, F=5.53 Hz at dimensionless times Ft=0.26, 0.46, 0.66, 0.86, 1.06, and 1.26

Re_C=350, and the flow field at this subcritical Reynolds number is steady. The flow field is identical from groove to groove. The outer channel flow moves essentially parallel to the x-direction with no significant transverse motion. Finally, the grooves are filled with slowly turning vortices.

Figure 5 shows streamlines for unsteadily forced flow at Re_m =267, η=0.4, and F=5.53 Hz. Streamlines are shown at six equally spaced dimensionless times, Ft=0.26, 0.46, 0.66, 0.86, 1.06, and 1.26 (see Eq. (1)) after periodic flow is established. The streamlines at each time are essentially symmetric about the channel centerline, and the flow field is identical from groove to groove. The flow in the grooves is not strongly separated at Ft =0.26, which is just after the maximum flow rate is reached. It exhibits only small vortices on the leeward surface of each groove. For $0.26<Ft<0.86$ the flow rate decelerates and then begins to re-accelerate. During this period these vortices grow and their centers move downstream. The vortices essentially disappear at Ft=1.08 when the flow begins to strongly accelerate. We see that modulating the flow rate under these conditions clears away the slowly turning groove vortices observed in Fig. 4.

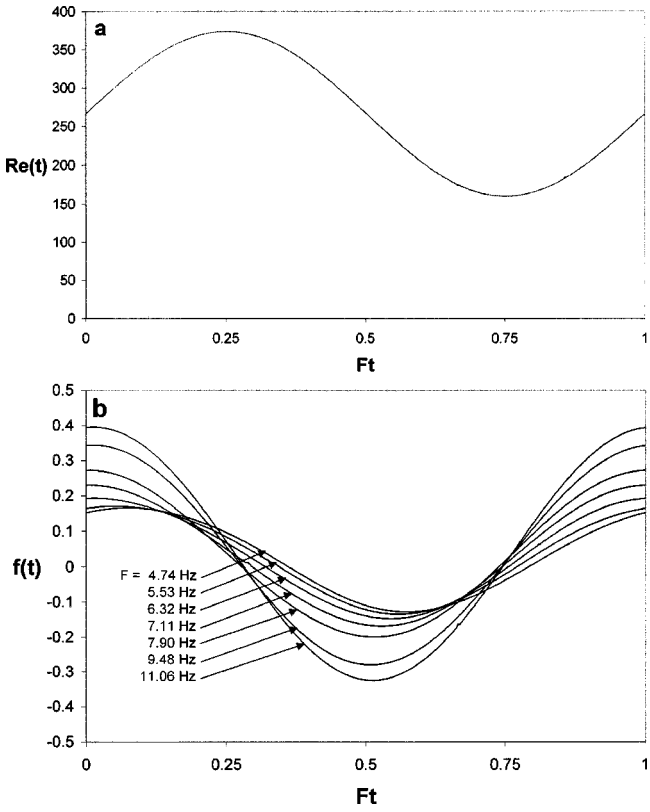

Fig. 6 (*a*) Reynolds number and (*b*) fanning friction factor versus dimensionless time for Re=267, η=0.4

Figures 6(*a*) and 6(*b*) show the time dependent Reynolds number and Fanning friction factor versus dimensionless time for Re_m=267, η=0.4 and a range of forcing frequencies 4.74 Hz $<F<$11.06 Hz. The time dependent Reynolds number versus dimensionless time varies sinusoidally and is identical for all seven forcing frequencies. The friction factor based on time dependent pressure gradient is defined as

$$f(t)=\left[-\frac{dp}{dx}(t)\right]\frac{D_h}{2\rho\overline{U}_m^2}=f_x(t)\,\frac{D_h^3}{2\,\mathrm{Re}_m^2\nu^2} \tag{5}$$

In this expression, $\overline{U}_m$ is the time average value of U_m, and $f_x(t)=(-dp/dx)/\rho$ is the time dependent body force, which is determined within the simulation so that the flow rate will follow the prescribed variation. The variation of the friction factor is nearly sinusoidally with time. The amplitude of the friction factor oscillation clearly increases with forcing frequency. Careful examination of Fig. 6(*b*) shows that the time mean value also increases with F. The phase shift between the friction factor and Reynolds number (flow rate) increases with forcing frequency as well. For $F\geqslant$6.32 Hz, the phase shift is nearly one quarter of the oscillatory period, corresponding to a phase angle of nearly $\pi/2$.

Because the flow rate varies with time, the pumping power required to modulate the flow also varies during the forcing cycle. The pumping power per unit volume is $(U_m)(-dp/dx)$. Figure 6(*b*) shows that $f(t)$ (and hence the pressure gradient $-dp/dx$) is positive and negative during different portions of the oscillatory period. Power must be supplied *to* the flow during periods when $(-dp/dx)>0$, and may be extracted *from* the flow when $(-dp/dx)<0$. The dimensionless *time-average* pumping power quantifies the *net* power input required from an external prime mover. This quantity is defined as:

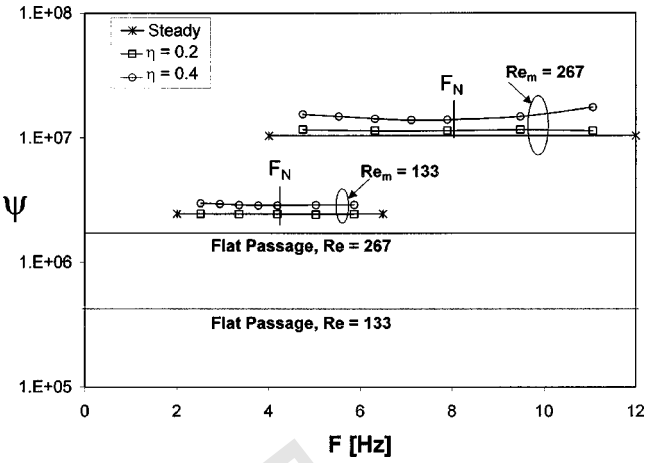

Fig. 7 Dimensionless pumping power versus forcing frequency, Reynolds number and oscillatory fraction

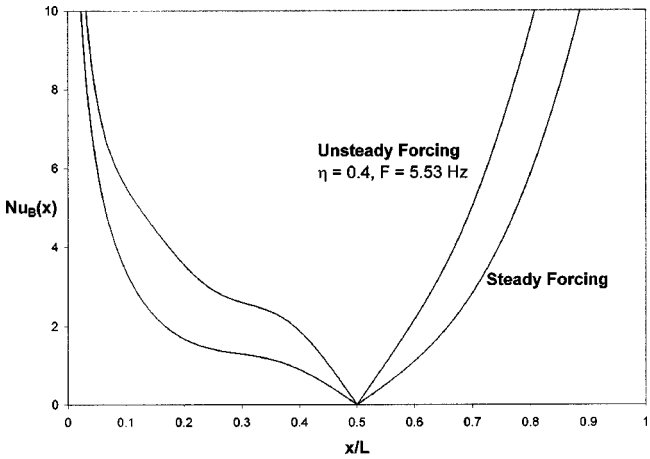

Fig. 8 Spatial variation of local bulk Nusselt number at Re_m =267 with steady and unsteady forcing

$$\Psi = -\frac{F}{\rho}\left(\frac{D_h}{v}\right)^3 \int_0^{1/F} \frac{dp}{dx}(t) V_N(t)\, dt$$

$$= \mathrm{Re}_m^2 \int_0^{Ft=1} f(Ft)\,\mathrm{Re}(Ft)\, d(Ft) \qquad (6)$$

The second equality in this expression shows that the dimensionless pumping power may be evaluated by time integrating the product of the friction factor and Reynolds number data presented in Fig. 6. The phase shift between Re(t) and $f(t)$ therefore affects the integration.

Figure 7 shows the dimensionless time-average pumping power versus forcing frequency at Re_m=133 and 267. Results are presented for η=0 (steady forcing), 0.2 and 0.4. Results are also presented for a flat passage (using f=24/Re_m in Eq. (6)). For steadily forced flow (η=0) the grooved passage pumping power is roughly six times larger than the flat passage level for both Re_m=133 and 267. The smaller minimum wall-to-wall spacing in the grooved channel causes this.

At Re_m=267, the pumping powers at and η=0.4 is roughly 40 percent higher than that for steady flow. However, the pumping power is minimized at $F \cong 7.5$ Hz. Figure 6 showed that both the amplitude and mean value of $f(t)$ increase with forcing frequency. However, the *phase shift* between $f(t)$ and Re(t) causes the net power requirement to decrease as F increases for $F<7.5$ Hz, and then increase at higher forcing frequencies. At Re_m=267 and η =0.2, the net pumping power is roughly 11 percent higher steadily forced flow, but it is minimized at $F \cong 6.3$ Hz. The forcing frequencies that minimize the pumping power are somewhat smaller than the predicted resonant frequency of F_N=8.04 Hz. Nonlinear effects at finite oscillatory fractions may cause the lower frequency. At Re_m=133, the pumping power at η=0.4 is roughly 20 percent higher than that for steadily forced flow. The minimum pumping power is at F=4 Hz, which is also somewhat lower than the predicted value of F_N=4.24 Hz. For η=0.2 the pumping power is within 1 percent of that for steady forcing.

The pumping power data presented in Fig. 7 represent the minimum input from a prime mover if *all* the work extracted during periods of $(-dp/dx)<0$ is delivered back to the flow during periods of $(-dp/dx)>0$. A flexible bladder or cylinder/flywheel device may be able to extract some energy from the flow and deliver it back at appropriate times in the cycle. However, friction and finite speed will not allow this device to operate reversibly. The net energy input for a real device will depend on the design of an energy storage and return system. The net pumping power levels reported in Fig. 7 represent a lower limit for a reversible system.

Figure 8 shows the spatial variation of the local Nusselt number for Re_m=267 for steady forcing η=0 and for unsteady forcing with η=0.4 and F=5.53 Hz. Results from all four grooves are plotted in the figure but essentially overlap. The local Nusselt number is based on the hydraulic diameter and projected surface area and defined as:

$$\mathrm{Nu}(x) = \frac{-\dfrac{dT_m}{d\hat{n}}(x)}{T_b(x)} \frac{D_h}{s} \qquad (7)$$

In this expression, the temperature gradient is evaluated in the direction normal to the wall and the wall direction cosine is s =0.7071. The local bulk temperature is

$$T_b(x) = \frac{\int u_m(x,y) T_m(x,y)\, dy}{\int u_m(x,y)\, dy} \qquad (8)$$

where $u_m(x,y)$ and $T_m(x,y)$ are the local velocity and temperature time averaged over one forcing cycle, and both integrals are evaluated from the top to the bottom of the domain.

The heat transfer on the windward surface of the groove ($0.5 \leqslant x/L \leqslant 1$) is significantly greater than that on the leeward face ($0 \leqslant x/L \leqslant 0.5$) for both steady and unsteady forcing. This is caused by the rotation direction of the groove vortex. The inflection at x/L=0.3 is caused by the impingement of the groove vortex at that location. The strong clearing of the fluid from the groove at η=0.4 and F=5.53 Hz (seen in Fig. 5) causes the heat transfer at all locations to be significantly higher than for steady forcing.

Figure 9 shows the log-mean Nusselt number versus forcing frequency at Re_m=133 and 267. Grooved channel results are presented for η=0 (steady forcing), 0.2 and 0.4. The flat passage Nusselt number Nu_{LM}=7.54 is based on laminar flow ($Re_m \leqslant 2800$). The natural frequencies predicted from linear stability theory are also shown. The log-mean Nusselt number is based on the projected surface area and the mean hydraulic diameter and is defined as

$$\mathrm{Nu}_{LM} = \frac{QD_h}{A_p T_{LM} k} = \mathrm{Re}_m \mathrm{Pr} \frac{Hc}{2} \qquad (9)$$

In this expression, the total heat transfer rate per unit length normal to the plane of Fig. 1 is $Q=\rho V_N[T_{B(x=0)}-T_{B(x=Ld)}]$, the projected surface area per unit length normal to the plane is A_p $=2L_d$, and the log mean temperature difference is T_{LM} $=[T_{B(x=0)}-T_{B(x=Ld)}]/\ln[T_{B(x=0)}/T_{B(x=Ld)}]=[T_{B(x=0)}-T_{B(x=Ld)}]/cL_d$, (note that $T_{B(x=0)}/T_{B(x=Ld)}=e^{cL_d}$, where c is the eigen decay rate constant described in the numerical methods section).

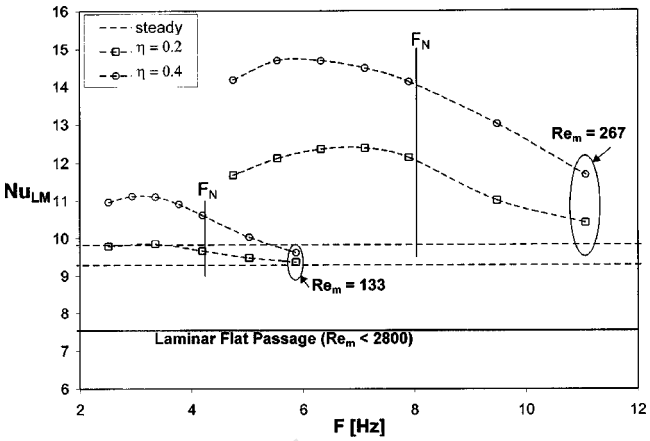

Fig. 9 Log-mean Nusselt number versus forcing frequency, Reynolds number and oscillatory fraction

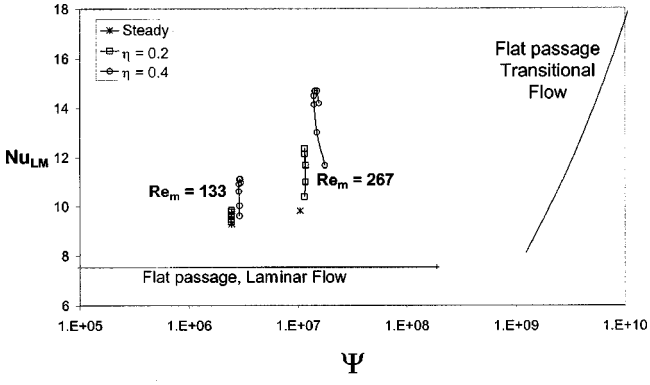

Fig. 10 Log-mean Nusselt number versus dimensionless pumping power

For steady forcing ($\eta=0$) the grooved passage Nusselt number increases with Reynolds number even though the laminar flat passage value is constant. The steadily forced grooved channel Nusselt numbers at Re=133 and 267 are 23 percent and 30 percent above the flat passage value, respectively.

The heat transfer exhibits a resonant response to oscillatory forcing and peaks at forcing frequencies that are somewhat below the values predicted from Orr-Sommerfeld theory. Table 1 summarizes the peak enhancement factors for different unsteady forcing conditions. For Re=267, the peak heat transfer with $\eta=0.4$ is at $F=6$ Hz and is 50 percent above the steadily forced value. The peak with $\eta=0.2$ is at $F=6.7$ Hz and is 26 percent above the steadily force case. For Re=133, the peak heat transfer with $\eta=0.4$ is 20 percent above the steadily forced value and is at $F=3.1$ Hz. The peak with $\eta=0.2$ is 6 percent above and is at $F=3.3$ Hz. By comparison, resonance in a sparsely grooved passage at $Re_m=1400$ with $\eta=0.2$ increases the heat transfer by 100 percent [4,12]. These data show that the maximum heat transfer enhancement factors increase with Reynolds number and with oscillatory fraction.

Figure 10 shows the log-mean Nusselt number versus net reversible pumping power for $Re_m=133$ and 267. Results at each Reynolds number are given for $\eta=0$ (steadily forced flow), 0.2 and 0.4. Comparisons are also made to flat passage results in the laminar and transitional regimes. For a flat passage the flow is laminar up to $Re_m=2800$ and the fully developed Nusselt number is independent of Reynolds number. At $Re_m=2800$ the dimensionless pumping power is $\Psi=Re_m^3 f=1.88\times10^8$ (where $f=24/Re_m$). In the transition region $Re_m>3000$, the Nusselt number increases with Reynolds numbers and hence with pumping power [25].

Grooved passage heat transfer levels are significantly higher than those in flat passages for the same pumping power. Since the flat passage laminar Nusselt number is independent of Reynolds number, a plane channel needs to operate in the transitional regime to reach the Nusselt numbers calculated for a steadily forced ($\eta=0$) grooved channel. Figure 10 shows that a flat passage operating in the transitional regime requires significantly more pumping power than a grooved passage operating at a low Reynolds number. Oscillatory forcing greatly increases the grooved passage heat transfer with only minor changes in the pumping power. At $Re_m=267$, oscillatory forcing with $\eta=0.4$ nearly doubles the heat transfer compared to flat passage flow with no increase in net reversible pumping power costs. Alternately, to reach a heat transfer level of $Nu_{LM}=10$, oscillatory flow in a grooved passage required *two orders of magnitude* less pumping power that a flat passage systems. This conclusion is based on a reversible energy extraction and delivery system. Oscillatory forcing requires special plumbing systems and increases the complexity of the prime mover. However, it appears to be a very effective method of increasing heat transfer in low Reynolds numbers systems such as micro-channels, especially if prime mover pumping power is limited.

Table 1 Peak enhancement factors for different mean Reynolds numbers and oscillatory fractions

Re_m	η	$Nu_{max}/Nu_{\eta=0}$
267	0.4	1.50
267	0.2	1.26
133	0.4	1.20
133	0.2	1.06

Conclusions

The effect of flow rate modulation on hydrodynamic resonance and heat transfer enhancement in a transversely grooved passage was numerically simulated using a two-dimensional spectral element technique. Linear stability theory was used to estimate the natural frequency that maximizes the effect on transport. Simulations were performed at moderately low mean Reynolds numbers of $Re_m=133$ and 267, with 20 percent and 40 percent flow rate oscillations.

The pumping power required to modulate the flow rate at given oscillatory amplitude was *minimized* as the forcing frequency approached the natural frequency. However, the flow mixing and heat transfer levels both *increased* as the natural frequency was approached. Hydrodynamic resonance enhances heat transfer at Reynolds numbers as low as $Re_m=133$, which is applicable to micro heat transfer devices. However, as the Reynolds number decreases, the oscillatory fraction required for a given enhancement factor increases.

Flat passages need to operate in the transitional regime ($Re_m>3000$) to achieve the heat transfer levels calculated for grooved passages at Re=133 or 267. As a result, oscillatory forcing in a grooved passage requires two *orders of magnitude* less pumping power than flat passage systems for the same heat transfer level. Oscillatory forcing may require special plumbing systems and increase the complexity of the prime mover. However, it appears to be an effective method of increasing heat transfer in low Reynolds number systems such as micro channels, especially when the pumping power is limited.

Acknowledgments

This work was supported in part by the Mathematical, Information, and Computational Sciences Division subprogram of the Office of Advanced Scientific Computing Research, U.S. Department of Energy, under Contract W-31-109-Eng-38.

Nomenclature

c = decay constant
D_h = hydraulic diameter, $2H$
F = dimensional frequency
F_N = dimensional natural frequency predicted from linear stability theory
f = fanning pressure gradient
f_x = fluid body force per unit mass in the x-direction
G = dimensional growth rate
H = mean channel wall-to-wall spacing
$H_{\max}$ = maximum channel wall-to-wall spacing
$H_{\min}$ = minimum channel wall-to-wall spacing
k = fluid thermal conductivity, 0.0263 W/m° C
K = number of spectral elements
L = groove length
L_d = domain length
N = spectral element order
Nu_b = bulk Nusselt number based on projected area
Pr = fluid molecular Prandtl number, 0.70
$\mathrm{Re}(t)$ = time dependent Reynolds number, $U_m(t)D_h/\nu$
Re_C = critical Reynolds number
Re_m = time mean Reynolds number
t = time
T = temperature
T_b = bulk temperature
u, v = velocity components in the x and y-directions
$U_m(t)$ = time dependent mean x-velocity at the mean channel cross-section
$\overline{U_m}$ = time average value of U_m
$U_{\max}$ = maximum x-velocity at the mean cross-section
V_N = volumetric flow rate per unit channel width

Greek

α = dimensionless wave number
α_t = thermal diffusivity, 2.63×10^{-5} m^2/s
ν = fluid kinematic viscosity, 1.84×10^{-5} m^2/s
η = oscillatory fraction
ψ = dimensionless pumping power per unit volume
θ = periodic temperature
ρ = fluid Density, 1.006 kg/m^3
τ = period of local time variations
Ω = computation domain
Ω_i = dimensionless growth rate
Ω_r = dimensionless natural frequency

References

[1] Peng, X. F., and Peterson, G. P., 1996, ''Convective Heat Transfer and Flow Friction for Water Flow in Microchannel Structures,'' Int. J. Heat Mass Transf., **39**, pp. 2599–2608.
[2] Rao, P., and Webb, R. L., 2000, ''Effects of Flow Mal-Distribution in Parallel Micro-Channels,'' *Proceedings of the ASME 34th National Heat Transfer Conference*, Pittsburgh Pa, August 20–22, Paper Number NHTC-2000 12102.
[3] Webb, R. L., 1994, *Principles of Enhanced Heat Transfer*, John Wiley and Sons, New York.
[4] Ghaddar, N. K., Korczak, K., Mikic, B. B., and Patera, A. T., 1986, ''Numerical Investigation of Incompressible Flow in Grooved Channels. Part 1: Stability and Self-Sustained Oscillations,'' J. Fluid Mech., **168**, pp. 541–567.
[5] Greiner, M., 1991, ''An Experimental Investigation of Resonant Heat Transfer Enhancement in Grooved Channels,'' Int. J. Heat Mass Transf., **24**, pp. 1383–1391.
[6] Roberts, E. P. L., 1994, ''A Numerical and Experimental Study of Transition Processes in an Obstructed Channel Flow,'' J. Fluid Mech., **260**, pp. 185–209.
[7] Kozlu, H., Mikic, B. B., and Patera, A. T., 1988, ''Minimum-Dissipation Heat Removal by Scale-Matched Flow Destabilization,'' Int. J. Heat Mass Transf., **31**, pp. 2023–2032.
[8] Karniadakis, G. E., Mikic, B. B., and Patera, A. T., 1988, ''Minimum-Dissipation Transport Enhancement by Flow Destabilization: Reynolds Analogy Revisited,'' J. Fluid Mech., **192**, pp. 365–391.
[9] Amon, C. H., Majumdar, D., Herman, C. V., Mayinger, F., Mikic, B. B., and Sekulic, D. P., 1992, ''Experimental and Numerical Investigation of Oscillatory Flow and Thermal Phenomena in Communicating Channels,'' Int. J. Heat Mass Transf., **35**, pp. 3115–3129.
[10] Greiner, M., 1987, ''Flow Field Destabilization and Heat Transfer Enhancement in Grooved Channels,'' *Forum on Unsteady Flow Separation*, ASME Applied Mechanics, Bioengineering, and Fluids Conference, Cincinnati, Ohio, June 14–17, FED-Vol. 52, ASME, New York, pp. 131–138.
[11] Greiner, M., Chen, R.-F., and Wirtz, R. A., 1990, ''Heat Transfer Augmentation Through Wall-Shaped-Induced Flow Destabilization,'' ASME J. Heat Transfer, **112**, pp. 336–341.
[12] Greiner, M., Chen, R.-F., and Wirtz, R. A., 1991, ''Enhanced Heat Transfer/Pressure Drop Measured From a Flat Surface in a Grooved Channel,'' ASME J. Heat Transfer, **113**, pp. 498–500.
[13] Greiner, M., Spencer, G., and Fischer, P. F., 1998, ''Direct Numerical Simulation of Three-Dimensional Flow and Augmented Heat Transfer in a Grooved Channel,'' ASME J. Heat Transfer, **120**, pp. 717–723.
[14] Greiner, M., Faulkner, R. J., Van, V. T., Tufo, H. M., and Fischer, P. F., 2000, ''Simulations of Three-Dimensional Flow and Augmented Heat Transfer in a Symmetrically Grooved Channel with Constant Temperature Walls,'' ASME J. Heat Transfer, **122**, pp. 653–660.
[15] Wirtz, R. A., Huang, F., and Greiner, M., 1999, ''Correlation of Fully Developed Heat Transfer and Pressure Drop in a Symmetrically Grooved Channel,'' ASME J. Heat Transfer, **121**, pp. 236–239.
[16] Lee, B. S., Kang, I. S., and Lim, H. C., 1999, ''Chaotic Mixing and Mass Transfer Enhancement by Pulsatile Laminar Flow in an Axisymmetric Wavy Channel,'' Int. J. Heat Mass Transf., **42**, pp. 2571–2581.
[17] Fox, R. W., and McDonald, A. T., 1985, *Introduction to Fluid Mechanics*, 3rd ed., John Wiley and Sons, New York.
[18] Drazin, P. G., and Reid, W. H., 1981, *Hydrodynamic Stability*, Cambridge University Press, London.
[19] Patera, A. T., 1984, ''A Spectral Element Method for Fluid Dynamics; Laminar Flow in a Channel Expansion,'' J. Comput. Phys., **54**, pp. 468–488.
[20] Maday, Y., and Patera, A. T., 1989, ''Spectral Element Methods for the Navier-Stokes Equations,'' *State of the Art Surveys on Computational Mechanics*, A. K. Noor and J. T. Oden, eds., ASME, New York, pp. 71–143.
[21] Fischer, P. F., 1997, ''An Overlapping Schwarz Method for Spectral Element Solution of the Incompressible Navier-Stokes Equations,'' J. Comput. Phys., **133**, pp. 84–101.
[22] Fischer, P. F., and Patera, A. T., 1992, ''Parallel Spectral Element Solutions of Eddy-Promoter Channel Flow,'' *Proceedings of the European Research Community on Flow Turbulence and Computation Workshop*, Lausanne, Switzerland, Cambridge University Press, pp. 246–256.
[23] Patankar, S. V., Liu, C. H., and Sparrow, E. M., 1977, ''Fully Developed Flow and Heat Transfer in Ducts Having Streamwise Periodic Variations of Cross-Sectional Area,'' ASME J. Heat Transfer, **99**, pp. 180–186.
[24] Kays, W. M., and Crawford, M. E., 1993, *Convection Heat and Mass Transfer*, third ed., McGraw-Hill, New York.
[25] Incropera, F. P., and DeWitt, D. P., 1996, *Introduction to Heat Transfer*, 3rd ed., John Wiley and Sons, New York.
[26] Fischer, P. F., and Patera, A. T., 1991, ''Parallel Spectral Element Solutions of the Stokes Problem,'' J. Comput. Phys., **92**, pp. 380–421.